

Flexible Spectral Methods for the Generation of Random Fields with Power-Law Semivariograms¹

Johannes Bruining,² Diederik van Batenburg,³
Larry W. Lake,⁴ and An Ping Yang⁵

Random field generators serve as a tool to model heterogeneous media for applications in hydrocarbon recovery and groundwater flow. Random fields with a power-law variogram structure, also termed fractional Brownian motion (fBm) fields, are of interest to study scale dependent heterogeneity effects on one-phase and two-phase flow. We show that such fields generated by the spectral method and the Inverse Fast Fourier Transform (IFFT) have an incorrect variogram structure and variance. To illustrate this we derive the prefactor of the fBm spectral density function, which is required to generate the fBm fields. We propose a new method to generate fBm fields that introduces weighting functions into the spectral method. It leads to a flexible and efficient algorithm. The flexibility permits an optimal choice of summation points (that is points in frequency space at which the weighting function is calculated) specific for the autocovariance structure of the field. As an illustration of the method, comparisons between estimated and expected statistics of fields with an exponential variogram and of fBm fields are presented. For power-law semivariograms, the proposed spectral method with a cylindrical distribution of the summation points gives optimal results.

KEY WORDS: random fields, permeability heterogeneity, fast Fourier transform, fractals, statistical properties.

INTRODUCTION

Random field generators are used widely as a tool to model heterogeneities in porous media (Lasseter, Waggoner, and Lake, 1986; Christakos, 1992; Pardo-Igúzquiza and Chico-Olmo, 1994) for applications in hydrocarbon recovery and groundwater flow. The generated field can be used as model (permeability) fields

¹Received 15 December 1995; revised 19 December 1996.

²Dietz Laboratory, Centre for Technical Geoscience, Mijnbouwstraat 120, 2628 RX Delft, Delft University of Technology, The Netherlands. e-mail: j.bruining@ta.tudelft.nl

³Halliburton B.V., European Research Centre, Leiderdorp, The Netherlands. e-mail: dbatenburg@halnet.com

⁴The University of Texas at Austin, Department Petroleum and Geosystems Engineering, e-mail: Larry-Lake@pgemailgate.pe.utexas.edu

⁵Texaco E & P Technology Division, P.O. Box 770070, Houston, Texas 77215-0070.

for research work (Waggoner, Castillo, and Lake, 1992). Prediction methods (King and others, 1993) for many realizations of such fields can quantify the uncertainty of expected product recoveries. Random fields can be conditioned to hard and soft data. (Hewett, 1986; Hewett and Behrens, 1990; Emanuel and others, 1989), for example collected from wells, to obtain sophisticated heterogeneity models of the field under consideration. Here, we critically evaluate the first step, that is the generation of unconditioned fields with a specific mean, variance, and autocovariance structure with long-range autocorrelations (with respect to the dimensions of the sample field). In particular we focus on random fields with a power-law variogram structure, also termed fractional Brownian motion (fBm) fields (Mandelbrot and Van Ness, 1968), which are of interest for example to study scale dependent dispersion effects.

A number of methods have been employed to generate random fields (Journel and Huijbregts, 1978; Deutsch and Journel, 1992). First, we note that all available methods generate correlated random fields from a sum of terms and hence generate approximately multi-Gaussian fields. Most earth-science phenomena are not multivariate Gaussian but can be transformed such that the resulting variable is approximately Gaussian for example the logarithm of the permeability (Jensen and Lake, 1988).

None of these methods have been evaluated critically as to their applicability to the generation of fields with power-law semivariograms. We briefly summarize here the limitations of the available methods. The Matrix Decomposition Method (Christakos, 1992; Yang, 1990) and Sequential Gaussian Simulation (Deutsch and Journel, 1992) require correlation functions. However, correlation functions for power-law variograms assume infinite values for points separated by finite distances. Limitations of dedicated spatial methods (for example, midpoint displacement method) to generate fBm fields are discussed extensively by Saupe (1988) and Voss (1988). The Turning Bands Method (TBM) (Yang, 1990; Mantoglou and Wilson, 1982; Mantoglou, 1987; Tompson, Ababou, and Gelhar, 1989) can be used in principle to generate 2-D fBm fields but the ensuing fields suffer from poor statistics (Bruining, 1992). Moreover, the TBM method is limited with respect to 3-D applications (Deutsch and Journel, 1992).

In this paper we investigate the applicability of spectral (Fourier) methods (Rice, 1954; Shinozuka and Jan, 1972; Saupe, 1988) to generate 2-D and 3-D fBm fields. fBm fields have a power-law semivariogram given by $\gamma(r) = \gamma_0 r^{2H}$ where r is the distance between points and H is the Hurst coefficient. The Hurst coefficient assumes values between zero (uncorrelated) and one (highly correlated). In order to assess the quality of the generated fBm fields we had to derive the prefactor in the spectral-density function for power-law variograms, which to our knowledge has not been presented previously. For our application visual

features “does it look like a natural landscape” (Voss, 1988) are not relevant to assess the quality of the generated fields. Indeed, the investigation was triggered by the observation that application of the Inverse Fast Fourier Transform (IFFT) algorithm to the spectral method (Saupe, 1988) leads to fields which have beautiful visual features but show poor agreement between expected and estimated statistics as calculated for each realization. We propose a new method to generate random fields. The method introduces weighting functions into the spectral (Fourier) method proposed by Shinozuka and Jan (1972). It leads to flexible and efficient algorithms. The flexibility permits an optimal selection of summation points (that is points in frequency space at which the weighting function is calculated) specific for the autocovariance structure of the field.

First, we describe the use of the generating equation with weighting functions. Then, we discuss briefly the algorithms used to generate the fields. Finally, in the numerical examples section we show comparisons between estimated and expected statistics of exponential and of fBm fields generated with different methods. For reasons of clarity we are concerned with aspects that involve mathematical derivations in the appendixes. In Appendix A we prove that the generating function with weighting functions leads to a field with the correct expected statistics. In Appendix B we derive some expected statistics of a sample Gaussian field such as the standard deviation of the average, the variance, and the standard deviation of the variance. In Appendix C we derive the prefactor for the spectral-density function for fBm. In Appendix D we derive the prefactor for fractional Gaussian noise (fGn) for reasons of easy reference. For the same reason we also give the 3-D spectral density functions of fBm and fGn in Appendix E. We limit our examples to 2-D situations in order to enable comparisons between many realizations without having to make use of excessive computer time.

GENERATING EQUATION

We propose the following modified generating equation (Shinozuka and Jan, 1972) of a random field value (symbol list at end of text)

$$f(x_1, x_2) = \sqrt{2} \sum_{k=1}^{N_1} \sum_{l=1}^{N_2} (S_2(\omega_{kl})w(\omega_{1k}, \omega_{2l}))^{1/2} \cos(\omega_{1k}x_1 + \omega_{2l}x_2 + \phi_{kl}) \quad (1)$$

for a two-dimensional field. The proof that Equation (1) gives a field with the correct expected statistical properties is given in Appendix A. In the equation, the indices 1, 2 denote the x - and y -direction. Application of Equation (1) requires further information on the phase angle ϕ_{kl} , the spectral-density function $S_2(\omega_{kl})$, the distribution of summation points and the weighting function $w(\omega_{1k}, \omega_{2l})$.

Table 1. Spectral-Density Functions

Semivariogram	2-D <i>sdf</i>	3-D <i>sdf</i>
Exponential		
$\gamma(s) = \sigma^2(1 - \exp(-s/\lambda))$	$S_2(\omega) = \frac{\sigma^2}{2\pi} \frac{\frac{1}{\lambda}}{\left(\omega^2 + \frac{1}{\lambda^2}\right)^{3/2}}$	$S_3(\omega) = \frac{\sigma^2}{\pi^2} \frac{\frac{1}{\lambda}}{\left(\omega^2 + \frac{1}{\lambda^2}\right)^2}$
fBm		
$\gamma(s) = \gamma_0 s^{2H}$	$S_2(\omega) = \frac{H^2 \gamma_0 2^{2H}}{\pi^2} \frac{\Gamma(H)^2 \sin(H\pi)}{\omega^{2H+2}}$	$S_3(\omega) = \frac{H\gamma_0}{2\pi\Gamma(1-2H)\cos(H\pi)} \frac{2H+1}{\omega^{2H+3}}$
fGn	Eq. (D1)	
$\gamma(s) = \gamma_0 \delta^{2H-2} - \frac{\gamma_0}{2\delta^2} \cdot ((s+\delta)^{2H} - 2s^{2H} + s-\delta ^{2H})$		$S_3(\omega) = \frac{H\gamma_0}{\pi^2 \omega^{2H+3} \delta^2} \Gamma(2H) \sin(H\pi) \cdot ((2H+1)(1-\cos(\omega\delta)) + \omega\delta \sin(\omega\delta))$

The random phase angle ϕ_{kl} is distributed uniformly between 0 and 2π . In the spectral-density function, denoted by $S_2(\omega_{kl})$, we use the abbreviation $\omega_{kl} = \sqrt{\omega_{1k}^2 + \omega_{2l}^2}$ and the subscript 2 to denote 2-D. A summary of spectral density functions for exponential (Mantoglou and Wilson, 1982) and fractal autocovariance structures is given in Table 1.

The distribution of summation points (see Fig. 1) ω_{1k}, ω_{2l} is determined by the requirement that the summation in Equation (A2) approximates the integral in Equation (A3). The highest frequencies ω_{1k}, ω_{2l} are practically bounded by the condition that contributions of terms with higher frequencies in the sum of Equation (1) would make negligible contributions. However Equation (1) represents, essentially, a Fourier transform. Consequently, we use frequencies ω_{1k}, ω_{2l} in the range $[-\pi/b, \pi/b)$ where b is the distance between points. We use the full autocorrelation structure of the field only if the integral of the spectral-density function over the thus-defined frequency space approaches σ^2 . In other words, it is only useful to generate a field with a certain autocorrelation structure if the points in space are distributed sufficiently densely such that they indeed contain the information on the complete spectral-density function (Press and others, 1992 p. 500). The preservation of the statistical properties depends only on having a sufficiently large number of points to get a reasonably distributed set of phase angles ϕ_{kl} at enough locations to accurately and completely sample the spectral density.

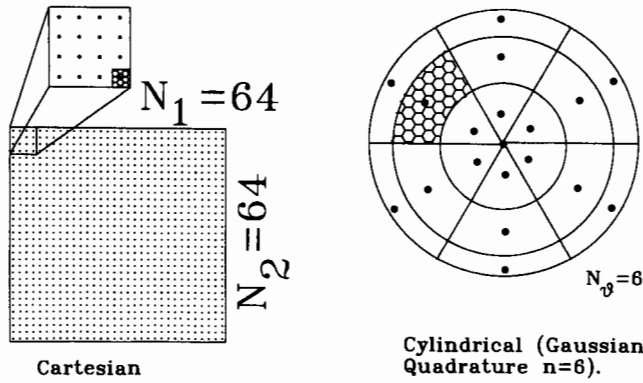


Figure 1. Two distributions of summation points in 2-D frequency space used in this article. Left, even distribution of summation points; right, cylindrical distribution. For cylindrical distribution, trapezoidal rule in angular and Gaussian quadrature in radial direction is used. For Gaussian quadrature, $n = 6$ (3 negative and 3 positive points on line through origin) instead of $n = 44$ points for reasons of illustration. Value of weights is proportional to enclosed area (see also Table 2).

An overview of weighting functions and the distribution of summation points used in this paper is given in Table 2. We distinguish between Cartesian (1) and Cylindrical (2) coordinates (see Fig. 1). We also tried a nonequidistant spacing in Cartesian coordinates (Bruining, 1992) but it produced poorer results. The indices k, l in Table 2 run from $[-N/2, N/2 - 1]$ (Cartesian). For the cylindrical configuration we need a summation over both the angular part and

Table 2. Examples of Weighting Functions and Distribution of Summation Points

Type	Weights $w(\omega_{1k}, \omega_{2l}) =$	Coordinates $(\omega_{1k}, \omega_{2l}) =$
Cartesian	$w_1(\omega_{1k})w_2(\omega_{2l}) = \Delta\omega_1\Delta\omega_2 = \frac{4\pi^2}{(bN)^2}$	$(\omega_{1k}, \omega_{2l}) = \left(\frac{2\pi k}{Nb}, \frac{2\pi l}{Nb}\right)$
		$k, l = -N/2, \dots, -1, 0, 1, \dots, N/2 - 1$
Cylindrical	$w_r(\omega_{kl})w_\theta(\theta_i) = \frac{2\pi\omega_{kl}}{N_\theta} w_r(\omega_{kl})$	$(\omega_{1k}, \omega_{2l}) = \left[\omega_{kl} \cos \frac{2\pi i}{N_\theta}, \omega_{kl} \sin \frac{2\pi i}{N_\theta}\right]$
	we use Gaussian quadrature for $w_r(\omega_{kl})$	$i = 0, 1, \dots, N_\theta - 1$

over the frequency part (see Table 2, Fig. 1). In Figure 1, the summation points are represented by dots, and weighting functions by the area. For Cartesian coordinates only one quadrant is shown.

COMPUTATIONAL ASPECTS

We use four different algorithms to generate the random fields. All algorithms, except for Sequential Gaussian Simulation (SGS), are in-house developed. SGS, as explained, is not suitable to generate fBm fields, but we will use SGS for comparison with the spectral methods as applied to exponential fields. The in-house developed algorithms are based on the solution of Equation (1). We distinguish two types of weighting functions.

Cartesian Weighting Functions

Equation (1) reduces to the original equation proposed by Shinozuka and Jan (1972) when we take the weighting function $w(\omega_{1k}, \omega_{2l})$ as being equal to the product of frequency spacings $\Delta\omega_1\Delta\omega_2$ in an equidistant grid pattern. For a square field with an equal number of points in each of the directions we may select $\Delta\omega_1 = \Delta\omega_2 = 2\pi/(bN)$ with $N = N_1 = N_2$ where Nb is equal to the system length (see Table 2). Expressions of weighting functions and weights are given in Table 2. With Cartesian weighting functions we apply both Inverse Fast Fourier Transform (IFFT) and (straightforward) Fourier summation (FT) to Equation (1). The difference between FT and IFFT lies in the fact that FT can use more points in frequency space than points in actual space at which we calculate the random field values. For the same number of frequency points as actual points FT and IFFT lead to identical results.

Cylindrical Weighting Functions

It is possible to express the weighting function $w(\omega_{1k}, \omega_{2l})$ in cylindrical coordinates (ω_{kl}, θ) as a product of two weighting functions that depend on the angle θ and the frequency ω_{kl} respectively (see Table 2). We restrict ourselves to the application of the trapezoidal rule to the angular dependent weighting function $w_\theta(\theta_i)$. The number of summations for $w_\theta(\theta_i)$ is denoted by N_θ . The ‘‘radial’’ dependent part w_r can be written as a product of the ‘‘radius’’ ω_{kl} and any weighting function $w_r(\omega_{kl})$ that is used for one-dimensional integration for example the trapezoidal rule, Simpson’s rule or Gauss-Legendre n -point quadrature formula (Press and others, 1992, p. 147–161) (see Table 2). Here we confine ourselves to the Gauss-Legendre n -point quadrature equations. The number of summations in the ‘‘radial’’ direction is denoted by N_r . Thus, we make

the substitution in Equation (1) $N_1 \rightarrow N_\theta$ and $N_2 \rightarrow N_r$. Calculations with cylindrical weighting functions is effective computationally with respect to FT but less effective than IFFT. However, as we shall show in the next section, IFFT leads to fields that show poor agreement between estimated and expected statistics. Moreover the cylindrical distribution of frequency points is flexible and allows the optimal choice dedicated to the correlation structure under consideration.

Random Number Generation

For an overview on the use of random number generators we refer to Press and others (1992, p. 274–286). The adage of their text is to be suspicious of system-supplied random number generators. We use their portable routine *ran3* which is based on a subtractive method.

NUMERICAL EXAMPLES

We apply the algorithms described to generate 64×64 random fields. All fields consist of 64×64 points to allow easy comparison to IFFT. Table 3 specifies the relevant parameters for the calculations. Our interest focusses on fractal fields. In order to illustrate the fields through a range of autocorrelation we calculated fGn fields (Mandelbrot and Van Ness, 1968, Appendix D) of $H = 0.51$ and 0.8 (both with $\delta = 3b$), and fBm fields (Appendix C) of $H = 0.2, 0.5,$ and 0.8 with the FT algorithm. Such a set can be used to study the effect of autocorrelation on displacement mechanisms. Figure 2 shows the plot of a single realization of each of the fractal fields. The trend from uncorrelated (erratic) behavior for fGn fields to the correlated (smooth) behavior of the fBm fields clearly is visible in spite of the fact that estimated statistical properties

Table 3. Parameters for Calculations^a

Coordinates	ω_{min}	ω_{max}	# Angular summations	Method
Cartesian	$\frac{\pi}{64b}$	$\frac{\pi}{b}$	128×128	IFFT
Cartesian	$\frac{\pi}{402b}$	$\frac{\pi}{b}$	402×402	Fourier (FT)
Cylindrical	$\frac{\pi}{64b}$	$\frac{\pi}{b}$	44×44	Trap. + Gauss.

^aSequential Gaussian Simulation (SGS) (Deutsch and Journel, 1992).

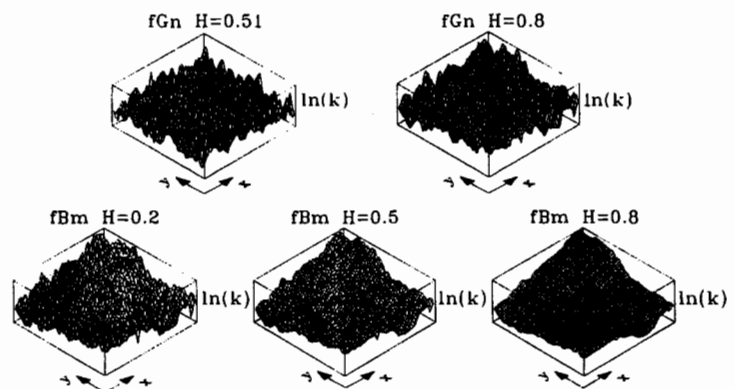


Figure 2. Plot of fractal fields for example logarithm of permeability; top: fGn fields with $H = 0.51$ and $H = 0.8$, bottom: fBm fields with $H = 0.2$, $H = 0.5$, and $H = 0.8$.

may deviate considerably from the expected properties. The fGn fields appear to be somewhat smoother because of the smoothing parameter $\delta = 3b$. The generation of fGn fields is as straightforward as the generation of, say, exponential fields once the spectral density function is known (see Appendix D).

Exponential Fields

We apply the four algorithms summarized in Table 3 to exponential fields. We use fields with an exponential autocovariance structure as a reference for conventional (nonpower-law) fields because it permits easy comparison to the programs provided by GSLIB (Deutsch and Journel, 1992). For Sequential Gaussian Simulation we use the input file (SGSIM.PAR) provided by GSLIB but adapt for a single exponential semivariogram with zero nugget. We use 100 realizations. For each of the 100 output fields with $\lambda = 4b$, $16b$, and $64b$ we calculate the omnidirectional semivariogram

$$\gamma(h) = \frac{1}{2N'} \sum_{i=1}^{N'} (f(\vec{x}_i) - f(\vec{x}_j))^2$$

where \vec{x}_i and \vec{x}_j denote points in the random field and N' the number of data, separated by a distance $h = |\vec{x}_i - \vec{x}_j|$. First we will compare the variograms and subsequently we will compare estimated vs. expected statistics of the generated fields.

Omnidirectional Variograms. Single realization omnidirectional semivariograms of a 64×64 fields are noisy. The reason for this is as follows: unidirectional semivariograms from single realizations of fields with long-range au-

tocorrelations are relatively smooth, because of the strong autocorrelations. However, these curves deviate substantially from the expected curves. Consequently, the curves in different directions also deviate considerably from each other. These deviations account for the ragged appearance of the omnidirectional semivariograms because the estimate fluctuates among variograms of different average directions when there are small changes in lag distance.

The noisiness decreases when more semivariograms of different realizations are averaged. The semivariograms obtained as an average of 100 realizations are somewhat ragged lines. The resulting average of 100 semivariograms is shown in Figure 3. In the figures the smooth line, which is the same in every column of the figure, is the expected semivariogram whereas the ragged lines are the estimated semivariograms. We observe that straightforward FT with (402

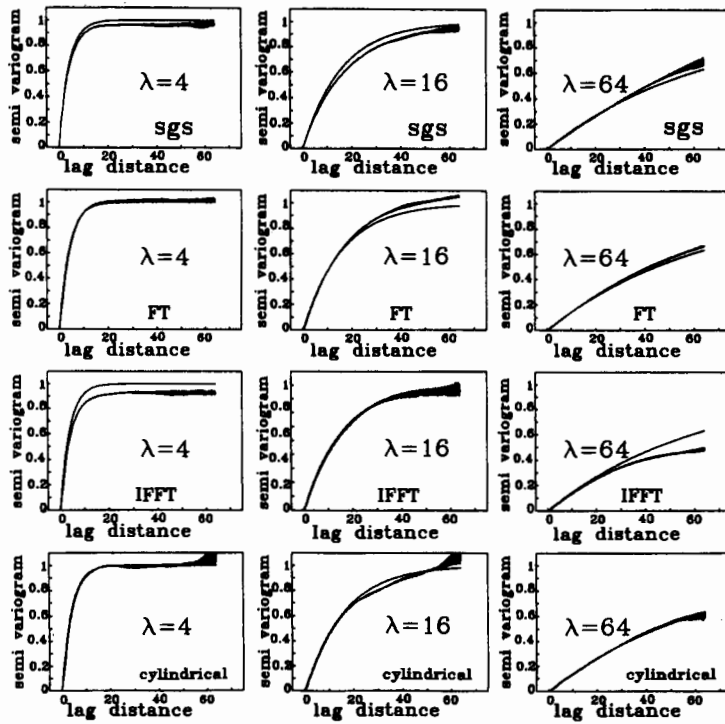


Figure 3. Omnidirectional semivariograms of exponential fields; averages of 100 realizations. Fields were obtained using parameters given in Table 3. Indicated in each figure are algorithm (FT, IFFT, etc.), autocorrelation length λ , expected (smooth) curves, and estimated (ragged) curves.

$\times 402$) frequency points shows good agreement. The quality of the field is at the expense of long computation times. IFFT generates a 128×128 field of which a quarter is retained. IFFT is extremely fast. There seems a small underestimate of the target variance for $\lambda = 4$ and $\lambda = 64$. A cylindrical distribution of frequency points yields acceptable results.

Unidirectional Variograms. We calculate the unidirectional semivariograms in the x -direction ([10]), and diagonal directions ([11] and [$\bar{1}\bar{1}$]) (see Kittel, 1986, for notation). The resulting average of 100 semivariograms is shown in Figure 4. The smoothest line is the expected semivariogram. The unidirectional semivariograms are more suitable for a critical evaluation of the algorithm used.

Statistics. The comparison of the estimated properties with the expected statistical properties of the field is useful for a further critical evaluation of the

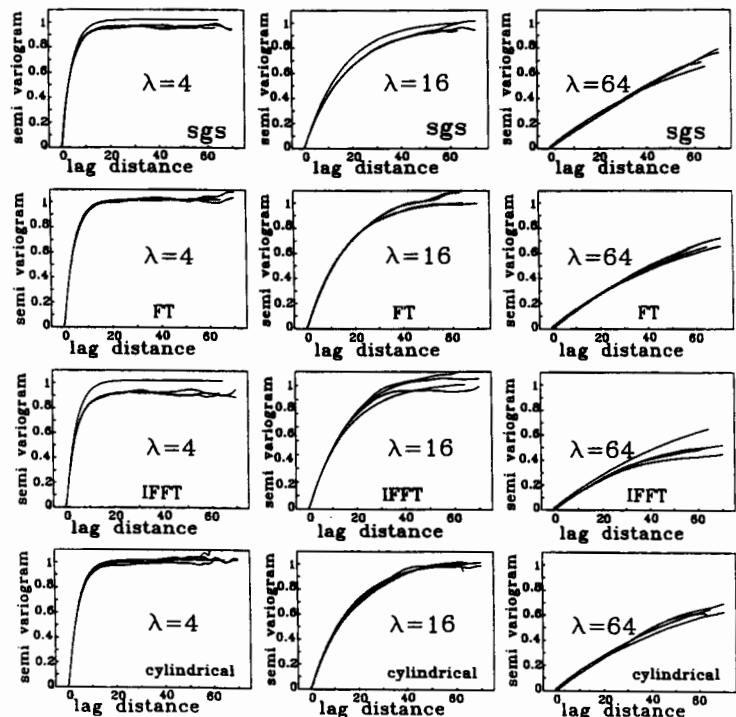


Figure 4. Unidirectional semivariograms of exponential fields; averages of 100 realizations. Fields were obtained using parameters given in Table 3. Indicated in each figure are algorithm (FT, IFFT, etc.), autocorrelation length λ , expected (smooth) curves, and three ([10], [11], [$\bar{1}\bar{1}$]) estimated (wiggling) curves.

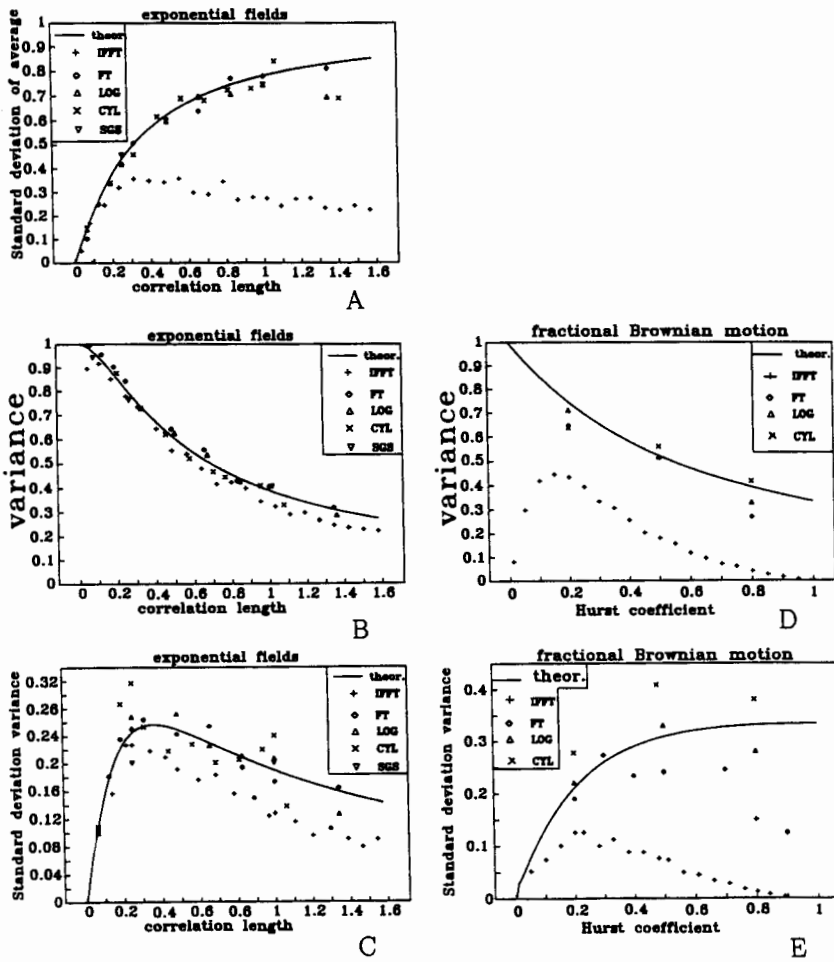


Figure 5. Statistics of exponential fields and power-law fields. A, compares expected standard deviation of average of exponential (sample) fields (line) to values estimated from fields generated using various algorithms as function of relative autocorrelation length; B, as A but now for sample variance; C, as A but now for standard deviation of sample variance; D, as B but now for fBm fields; E, as C but now for fBm fields. Counterpart of A for fBm fields is infinity.

different algorithms. Figure 5 compares the estimated properties and the expected properties. Inspection of Figure 5 also demonstrates the justification of averaging 100 realizations. For instance Figure 5C shows that the standard deviation of the variance of a single realization is about 0.25. Therefore, the standard deviation for 100 realizations is 0.025, corresponding to 95% confi-

dence limits of ± 0.05 for the variance as shown in Figure 5B. Appendix B derives the expressions for the expected statistical properties such as the standard deviation of the average, the variance and the standard deviation of the variance. Table 4 gives some of the statistical properties estimated from the sample fields.

Figure 5A–5C show that all algorithms, except IFFT, generate exponential fields that show fair agreement between the theoretical and the estimated statistical properties. Figure 5A shows that expected and estimated standard deviation of the average for IFFT disagree whereas all other methods are in agreement with the expected values. Similar behavior has been observed by Tompson, Ababou, and Gelhar, (1989). We note that a good simulation technique is not a technique that reproduces the expected values [as does simulated annealing (Deutsch and Journel, 1992)] but rather a technique that has the correct variations between realizations.

Figure 5B shows the estimated variance, which is in agreement with the expected variance for all methods considered. However, in Figure 5C the estimated standard deviation of the variance for the IFFT again is systematically lower than the expected value. All other methods show a scatter around the expected value. These conclusions are supported by the data presented in Table 4. However, for the skewness and kurtosis the standard deviations obtained with IFFT show agreement with the values obtained with the other methods. Note that the estimated kurtosis is negative (platykurtic). This underlines once again that it is impossible to measure statistics of the full field from measurements only (Jakeman and Jordan, 1990) taken on the finite field with long-range autocorrelations (Jensen and Lake, 1988).

Table 5 summarizes the performance of the different methods. Sequential Gaussian Simulation is the preferred algorithm for exponential fields for reasons of computational efficiency.

fBm Fields

We apply three algorithms to calculate fBm fields. The power-law model has infinite theoretical variance and consequently is not implemented in the sequential Gaussian simulation program of GSLIB (Deutsch and Journel, 1992). First, we will compare the variograms and subsequently we will compare estimated versus expected statistics of the generated fields.

Omnidirectional Variograms. The semivariogram of 100 realizations presented in Figure 6 shows that the FT algorithm with 402×402 frequency terms gives acceptable results. The estimated semivariogram, however, is lower than the expected semivariogram. Also, the algorithm is highly inefficient from a computational point of view. We observe that IFFT is not suitable to use to generate fields with power-law semivariograms. This algorithm, when implemented in commercial packages, is to be used for artistic landscape drawings

Table 4. Estimated Statistics of Fields; Average \pm Standard Deviation

Method	Covariance	Average	Variance	Skewness	Kurtosis
Cartesian (IFFT)	exp $\lambda = 4$	-0.00 \pm 0.14	0.99 \pm 0.10	-0.03 \pm 0.13	0.01 \pm 0.21
Cartesian (IFFT)	exp $\lambda = 16$	-0.04 \pm 0.26	0.79 \pm 0.23	0.03 \pm 0.30	-0.14 \pm 0.35
Cartesian (IFFT)	exp $\lambda = 64$	-0.04 \pm 0.25	0.33 \pm 0.13	0.04 \pm 0.36	-0.22 \pm 0.47
Cartesian (FT)	exp $\lambda = 4$	0.00 \pm 0.14	0.99 \pm 0.10	-0.02 \pm 0.13	0.01 \pm 0.21
Cartesian (FT)	exp $\lambda = 16$	-0.02 \pm 0.42	0.84 \pm 0.25	-0.02 \pm 0.29	-0.15 \pm 0.37
Cartesian (FT)	exp $\lambda = 64$	-0.10 \pm 0.78	0.40 \pm 0.17	-0.01 \pm 0.38	-0.27 \pm 0.50
Cylindrical	exp $\lambda = 4$	-0.09 \pm 0.14	0.99 \pm 0.11	0.02 \pm 0.13	-0.02 \pm 0.20
Cylindrical	exp $\lambda = 16$	-0.22 \pm 0.41	0.81 \pm 0.32	0.03 \pm 0.28	-0.21 \pm 0.38
Cylindrical	exp $\lambda = 64$	0.11 \pm 0.71	0.39 \pm 0.24	0.03 \pm 0.35	-0.35 \pm 0.49
Seq. Gauss	exp $\lambda = 4$	0.02 \pm 0.15	0.94 \pm 0.11	0.01 \pm 0.13	-0.02 \pm 0.18
Seq. Gauss	exp $\lambda = 16$	0.10 \pm 0.46	0.76 \pm 0.20	-0.02 \pm 0.25	-0.19 \pm 0.30
Seq. Gauss	exp $\lambda = 64$	0.16 \pm 0.75	0.40 \pm 0.20	-0.04 \pm 0.38	-0.27 \pm 0.55
Cartesian (IFFT)	fBm H = 0.2	-	0.43 \pm 0.11	0.02 \pm 0.25	-0.11 \pm 0.26
Cartesian (IFFT)	fBm H = 0.5	-	0.18 \pm 0.07	0.04 \pm 0.37	-0.23 \pm 0.48
Cartesian (IFFT)	fBm H = 0.8	-	0.04 \pm 0.02	0.04 \pm 0.44	-0.36 \pm 0.62
Cartesian (FT)	fBm H = 0.2	-	0.65 \pm 0.19	-0.01 \pm 0.25	-0.14 \pm 0.31
Cartesian (FT)	fBm H = 0.5	-	0.51 \pm 0.24	-0.02 \pm 0.38	-0.36 \pm 0.50
Cartesian (FT)	fBm H = 0.8	-	0.26 \pm 0.15	-0.03 \pm 0.45	-0.51 \pm 0.66
Cylindrical	fBm H = 0.2	-	0.64 \pm 0.28	0.03 \pm 0.23	-0.19 \pm 0.32
Cylindrical	fBm H = 0.5	-	0.56 \pm 0.41	0.03 \pm 0.36	-0.42 \pm 0.50
Cylindrical	fBm H = 0.8	-	0.41 \pm 0.38	0.03 \pm 0.40	-0.59 \pm 0.57

Table 5. Ratings of Statistical Properties for Generated Exponential and fBm Fields^a

Correlation structure	Characteristic	IFFT	FT	Cyl	SGS
Exponential	standard dev. of average variance	poor	good	good	good
	standard dev. of variance	good	good	good	good
	omni-dir. semivariogram	poor	good	fair	good
	uni-dir. semivariogram	fair	good	good	good
	computation time (rem)	poor	fair	fair	good
fBm	computation time (rem)	0.36"	50'	33"	10"
	variance	poor	good	good	NA
	standard dev. of variance	poor	fair	fair	NA
	omni-dir. semivariogram	poor	fair	good	NA
	uni-dir. semivariogram	poor	fair	fair	NA
	computation time (rem)	0.37"	50'	33"	NA

^aNA = not applicable. rem: user time for one single field calculation on HP 9000/735 @ 100 MHz and 128 Mb memory.

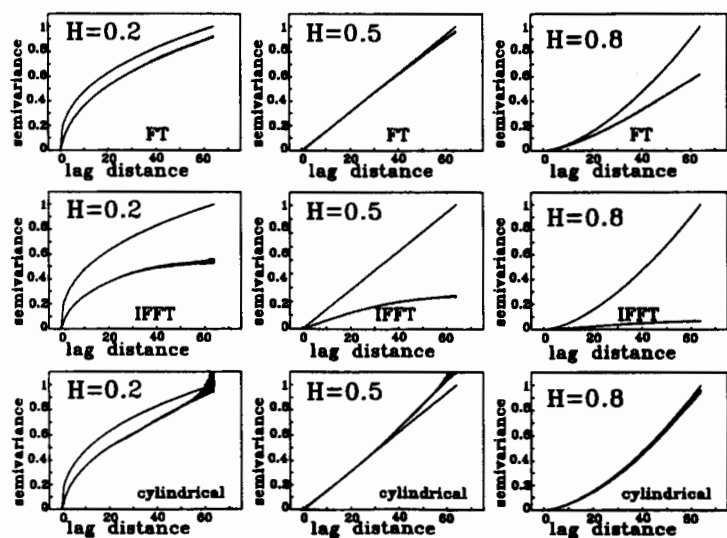


Figure 6. Omnidirectional semivariograms of fBm fields; averages of 100 realizations. Fields were obtained using parameters given in Table 3. Indicated in each figure are algorithm (FT, IFFT, etc.), Hurst coefficient H , expected (smooth) curves, and estimated (ragged) curves.

(Voss, 1988). Finally, a cylindrical distribution of frequency points leads to the best agreement between estimated and expected semivariograms for all values of the Hurst coefficient.

Unidirectional Variograms. We calculate the unidirectional semivariograms in the [10], [11], and [11̄] directions. The resulting semivariogram is presented in Figure 7. The smoothest line is the expected semivariogram. Again, the unidirectional semivariograms are more suitable for a critical evaluation of the algorithm used. The algorithm with a cylindrical distribution of frequency points shows excellent performance, also for low values of H . Considering the computation times, it is noted that 83.5 times fewer frequency points were used for the cylindrical distribution of frequency points than for the “full” Fourier transform.

Statistics. It should be noted that the average for fBm fields is meaningless, due to the infinite value of the lowest frequency part of the spectral density function ($S_2(\omega_{kl}) \rightarrow \infty$ as $\omega \rightarrow 0$). The expected standard deviation of the average is infinity. Finite values are observed only because we cut off (by our numerical procedure) the low-frequency part of the spectral density function.

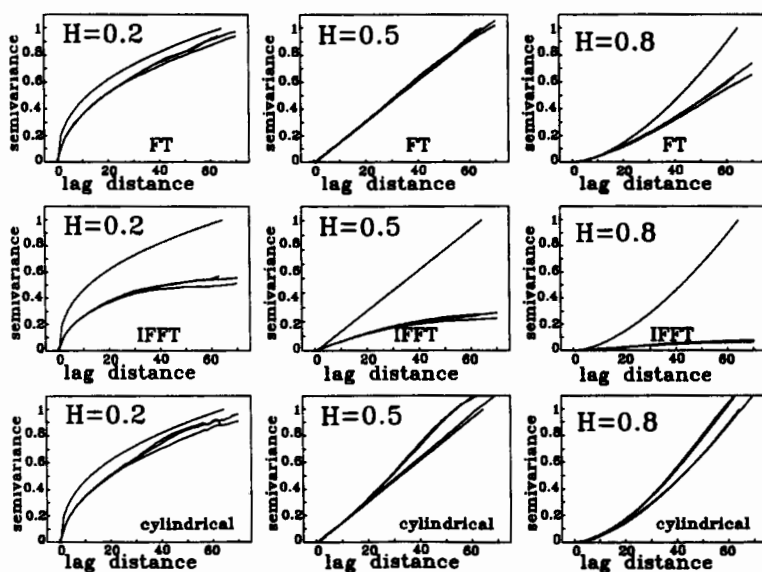


Figure 7. Unidirectional semivariograms of fBm fields; averages of 100 realizations. Fields were obtained using parameters given in Table 3. Indicated in each figure are algorithm (FT, IFFT, etc.), Hurst coefficient H , expected (smooth) curves, and three ([10], [11], [11̄]) estimated (wiggling) curves.

The low-frequency part, essentially, adds only a constant to all field values, which can be subtracted subsequently to obtain a valid realization.

We use again 100 fields with 64×64 points to obtain estimated values. The variance (with respect to the sample average) of fBm fields is finite (see Appendix B). The IFFT shows an estimated value of the variance which is systematically too low (see Figure 5D). This was expected in view of the low values of the semivariograms (see Figs. 6 and 7). Figure 5E compares the estimated and the expected values of the standard deviation of the variance. Again, the IFFT shows values for the standard deviation of the variance that are systematically too low. The other methods show scatter around the expected value indicating agreement between estimated and expected properties. The skewness of the fields (see Table 4) is zero which is expected for reasons of symmetry whereas the kurtosis is negative (platykurtic). The results, summarized in Table 5, show the cylindrical distribution of frequency points to be optimal. It is efficient from the computational point of view and it has superior statistical properties.

CONCLUSIONS

- Sequential Gaussian simulation is the preferred method for generating random fields with an exponential variogram. The method is efficient from the computational point of view. There is good agreement between the expected and the estimated statistics.
- The Inverse Fast Fourier Transform (IFFT) algorithm applied to the spectral method for exponential fields yields the correct estimated semi-variogram structure but fails to reproduce the expected standard deviation of both the average and the variance for fields with long-range correlations.
- The IFFT algorithm fails to generate fBm fields with the proper statistical properties.
- fBm fields obtained with the spectral method using a Fourier sum (FT) that involves a dense regular distribution of frequency points show good agreement between the expected and the estimated statistics. The algorithm is computationally expensive. When there is a sparser distribution of points, the algorithm converges to the same numerical equation as used for IFFT with the same inherent problems.
- fBm fields obtained using a spectral method that involves a cylindrical distribution of frequency points and the application of Gaussian quadrature is superior to FT. It is more efficient from the computational point of view and leads to superior statistical properties.

ACKNOWLEDGMENTS

Johannes Bruining's stay at The University of Texas at Austin was made possible by financial support from the Dutch Technology Foundation (STW). Further support came from the Enhanced Oil and Gas Recovery Research Program of the Center for Petroleum and Geosystems Engineering at The University of Texas. A research grant from Delft University of Technology for the project "Free boundary problems for multiphase flow in porous media" supplied the computer on which the simulations were carried out. Diederik van Batenburg would like to thank the management of Halliburton Energy Services for their support and permission to publish this work. J. B. thanks P. Bedrikovetskii and A. F. B. Tompson for useful discussions. We thank B. T. de Haas for close reading of the final test.

NOTATION

b	distance between neighboring points
$B(z_1, z_2)$	beta function for z_1, z_2
C	autocovariance function
$E[]$	expectation operator
$f(x_1, x_2)$	random 2-D field
${}_1F_2(a; b, c; z)$	hypergeometric series
$g(x_1, x_2, x_3)$	random 3-D field
h	distance between points
H	Hurst coefficient
L	length of sample field
N	number of summations in one direction
r	distance between points
\mathbf{r}	position of point in space
s	distance between points
S_i	i -D-spectral density function $i = 1, 2, 3$
x_i	x, y, z position for $i = 1, 2, 3$
Δx	spacing
$w(\omega_{1k}, \omega_{2l})$	weighting function (see Table 2)
Greek:	
γ	semivariogram
γ_σ	variance parameter for fBm
$\Gamma(z_1)$	gamma function for z_1
δ	smoothing parameter for fGn
$\Delta\omega$	frequency spacing

θ	angle in frequency space
λ	correlation length
μ	expected average
σ^2	variance
ϕ	random phase angle
ω	frequency
ω_{kl}	$\sqrt{\omega_{1k}^2 + \omega_{2l}^2}$
Subscripts:	
1	x-direction or 1-D
2	y-direction or 2-D
3	z-direction or 3-D
i	$i = 1, 2, 3$ direction index or summation index
k, l, m	frequency summation indexes
r	radial
θ	angular

REFERENCES

- Abramowitz, M., and Stegun, I., 1972, Handbook of mathematical functions (9th printing): Dover Publ., New York, 1046 p.
- Bruining, J., 1992, Modeling reservoir heterogeneity with fractals: Enhanced Oil and Gas Recovery Research Program, Rept. No. 92-5, Center for Petroleum and Geosystems Engineering, Univ. of Texas, Austin, 88 p.
- Christakos, G., 1992, Random field models in earth sciences: Academic Press, Hartcourt Brace Jovanovich Publ., San Diego, California, 474 p.
- Deutsch, C. V., and Journel, A. G., 1992, GSLIB; Geostatistical Software Library and user's guide: Oxford Univ. Press, New York, 340 p.
- Emanuel, A. S., Alameda, G. K., Behrens, R. A., and Hewett, T. A., 1989, Reservoir performance prediction methods based on fractal geostatistics: SPE Reservoir Engineering, v. 4, no. 3, p. 311-318.
- Gradshteyn, I. S., and Ryzhik, I. M., 1979, Table of integrals, series, and products: Academic Press, Hartcourt Brace Jovanovich Publ., San Diego, California, 1160 p.
- Hewett, T. A., 1986, Fractal distributions of reservoirs heterogeneity and their influence on fluid transport: SPE Paper 15386, SPE Reprint Series no. 27, Reservoir Characterization-2, p. 67-82.
- Hewett, T. A., and Behrens, R. A., 1990, Conditional simulation of reservoir heterogeneities with fractals: SPE Formation Evaluation, v. 5 no. 3, p. 217-225.
- Jakeman, E., and Jordan, D. L., 1990, Statistical accuracy of measurements on Gaussian fractals: Jour. Phys. D: Appl. Phys., v. 23, p. 397-405.
- Jensen, J. L., and Lake, L. W., 1988, The influence of sample size and permeability distribution on heterogeneity measures: SPE Reservoir Engineering, v. 3, no. 2, p. 629-637.
- Journel, A. G., and Huijbregts, C. J., 1978, Mining geostatistics: Academic Press, London, 600 p.
- Kampen, N. G. van, 1992, Stochastic processes in physics and chemistry (revised and enlarged edition): North Holland, Amsterdam, 465 p.
- King, M. J., Blunt, M. J., Mansfield, M., and Christie, M. A., 1993, Rapid evaluation of the

- impact of heterogeneity on miscible gas injection: Proc. 7th European Symp. on IOR, (Moscow, Russia), v. 2, p. 398–407.
- Kittel, C., 1986, Introduction to solid state physics: John Wiley & Sons, New York, 646 p.
- Lasseter, T. J., Waggoner, J. R., and Lake, L. W., 1986, Reservoir heterogeneity and its influence on ultimate recovery, in Lake, L. W., and Carroll, H. B., eds., Reservoir characterization: Academic Press, Orlando, Florida, 659 p.
- Mandelbrot, B. B., and Van Ness, R., 1968, Fractional Brownian motions, fractional noises and applications: SIAM review, v. 10, no. 4, p. 422–437.
- Mantoglou A., 1987, Digital simulation of multivariate two- and three-dimensional stochastic processes with a spectral turning bands method: Math. Geology, v. 19, no. 2, p. 129–149.
- Mantoglou, A., and Wilson, J. L., 1982, The turning bands method for simulation of random fields using the line integration by a spectral method: Water Resources Res., v. 18, no. 5, p. 1379–1394.
- Oberhettinger, F., 1990, Tables of Fourier transforms and Fourier transforms of distributions: Springer Verlag, Berlin, 259 p.
- Pardo-Igúzquiza, E., and Chica-Olmo, M., 1994, Spectral simulation of multivariate stationary random functions using covariance Fourier transforms: Math. Geology, v. 26, no. 3, p. 277–299.
- Press, W. H., Flannery, B. P., Teukolsky S. A., and Vetterling, W. T., 1992, Numerical recipes in C: Cambridge Univ. Press, New York, 994 p.
- Prudnikov, A. P., Brychkov, Yu. A., and Marichev, O. I., 1986, Integrals and series: Vol. 1, Elementary functions: Translated from the Russian by N. M. Queen Gordon, Breach Science Publ., New York, 798 p.
- Rice, S. O., 1954, Mathematical analysis of random noise, in Wax, N., ed., Selected papers on noise and stochastic processes: Dover Publ., New York, p. 133–294.
- Saupe, D., 1988, Algorithms for random fractals, in Peitgen, H. O., and Saupe, D., eds., The science of fractal images: Springer-Verlag, New York, 312 p.
- Shinozuka, M., and Jan, C. M., 1972, Digital simulation of random processes and its applications: Jour. Sound and Vibration, v. 25, no. 1, p. 357–368.
- Tompson, A. F. B., Ababou, R., and Gelhar, L. W., 1989, Implementation of the three-dimensional turning bands random field generator: Water Resources Res., v. 25, no. 10, p. 2227–2243.
- Tsuji, H., 1955, The transformation equations between one- and n -dimensional spectra in the n -dimensional vector or scalar fluctuation field: Jour. Phys. Soc. Japan, v. 10, no. 4, p. 278–285.
- Vanmarcke, E., 1983, Random field analysis and synthesis: M.I.T. Press, Cambridge, Massachusetts, 382 p.
- Voss, R., 1988, Fractals in nature: from characterization to simulation, in Peitgen, H. O., and Saupe, D., eds., The science of fractal images: Springer-Verlag, New York, 312 p.
- Waggoner, J. R., Castillo, J. L., and Lake, L. W., 1992, Simulation of EOR processes in stochastically generated permeable media, SPE Formation Evaluation, v. 7, no. 2, p. 173–180.
- Yang, A. P., 1990, Stochastic heterogeneity and dispersion: unpubl. doctoral dissertation, Univ. Texas, Austin, 242 p.
- Yang, A. P., and Lake, L. W., 1989, The Accuracy of autocorrelation estimates: In Situ, v. 12, no. 4, p. 227–274.

APPENDIX A. EXPECTED STATISTICS OF EQ. 1 FIELDS

Here we prove that Equation (1) leads to a 2-D field with the correct, expected statistical properties when weighting functions are introduced. First,

by virtue of the central limit theorem (Rice, 1954), the field values tend to be distributed normally when Equation (1) is applied. Second, the expected average value $E[f(x_1, x_2)] = 0$. Indeed, application of the expectation operator to Equation (1) gives

$$E[f(x_1, x_2)] = \sqrt{2} \sum_{k=1}^{N_1} \sum_{l=1}^{N_2} (S_2(\omega_{kl})w(\omega_{1k}, \omega_{2l}))^{1/2} \cdot E[\cos(\omega_{1k}x_1 + \omega_{2l}x_2 + \phi_{kl})] = 0$$

where we use the property that the expectation operator operates only on the terms which contain the random phase angle, and that the expectation of a cosine or a sine of a uniformly distributed random phase angle is zero.

Finally, we show that the expected autocorrelation function of the field $f(x_1, x_2)$ indeed approximates the Fourier cosine transform of the spectral density function:

$$E[f(x_1, x_2)f(x_3, x_4)] = 2 \sum_{k=1}^{N_1} \sum_{l=1}^{N_2} \sum_{m=1}^{N_1} \sum_{n=1}^{N_2} (S_2(\omega_{kl})w(\omega_{1k}, \omega_{2l})S_2(\omega_{mn}) \cdot w(\omega_{1m}, \omega_{2n}))^{1/2} E[\cos(\omega_{1k}x_1 + \omega_{2l}x_2 + \phi_{kl}) \cdot \cos(\omega_{1m}x_3 + \omega_{2n}x_4 + \phi_{mn})] \quad (A1)$$

The expectation of the product of the cosines is zero unless $\phi_{kl} = \phi_{mn}$, that is $k = m$ and $l = n$. We use the rule $2 \cos \alpha \cos \beta = \cos(\alpha + \beta) + \cos(\alpha - \beta)$ and obtain

$$E[\cos(\omega_{1k}x_1 + \omega_{2l}x_2 + \phi_{kl}) \cos(\omega_{1k}x_3 + \omega_{2l}x_4 + \phi_{kl})] \\ = \frac{1}{2} E[\cos(\omega_{1k}(x_1 + x_3) + \omega_{2l}(x_2 + x_4) + 2\phi_{kl})] \\ + \frac{1}{2} E[\cos(\omega_{1k}(x_1 - x_3) + \omega_{2l}(x_2 - x_4))]$$

The first term on the right side is again zero. The second term represents the expectation of a term without a random term and thus is equal to $\frac{1}{2} \cos(\omega_{1k}(x_1 - x_3) + \omega_{2l}(x_2 - x_4))$. Therefore, we can simplify Equation (A1)

$$E[f(x_1, x_2)f(x_3, x_4)] = \sum_{k=1}^{N_1} \sum_{l=1}^{N_2} S_2(\omega_{kl}) \cos(\omega_{1k}(x_1 - x_3) + \omega_{2l}(x_2 - x_4))w(\omega_{1k}, \omega_{2l}) \quad (A2)$$

The autocorrelation function $E[f(x_1, x_2)f(x_3, x_4)]$ must approach the Fourier cosine transform of the spectral density function. Hence, we must have

$$E[f(x_1, x_2)f(x_3, x_4)] \approx \int_{-\infty}^{\infty} \int_{-\infty}^{\infty} S_2(\omega_{kl}) \cos(\omega_1(x_1 - x_3) + \omega_2(x_2 - x_4)) d\omega_1 d\omega_2 \tag{A3}$$

This shows that whenever the sum in Equation (A2) approaches the integral in Equation (A3) the generated field is expected to approach the correct autocovariance structure. When the appropriate weighting functions are introduced, Equation (A2) is a numerical approximation of Equation (A3). Therefore, the fields generated with Equation (1) approach a Gaussian field with a zero mean and a given autocovariance structure. Such a field is statistically uniquely defined (Kampen, 1992). This completes our proof.

The generating equation of a random field value for a three-dimensional field is

$$g(x_1, x_2, x_3) = \sqrt{2} \sum_{k=1}^{N_1} \sum_{l=1}^{N_2} \sum_{m=1}^{N_3} (S_3(\omega_{klm})w(\omega_{1k}, \omega_{2l}, \omega_{3m}))^{1/2} \cdot \cos(\omega_{1k}x_1 + \omega_{2l}x_2 + \omega_{3m}x_3 + \phi_{klm}) \tag{A4}$$

The proof that Equation (A4) leads to a field with the correct expected statistical properties is analogous completely to the 2-D situation.

APPENDIX B. STATISTICAL PROPERTIES OF FINITE FIELDS

The expected properties of finite fields are not always the same as the properties of infinite fields if the values are compared to the sample averages of the finite fields. For example, the expected variance of a fBm (infinite) field is infinite. However, the estimated variance of a sample fBm field is never infinite as the values are likely to be similar to the sample average values in the highly autocorrelated fields. In general, the variance of a finite field (with respect to the sample average) is smaller than the expected variance of an infinite field. Also, the sample average can deviate considerably from the expected mean and will be different for each realization. The expected variance of the sample mean is infinite for fBm fields but finite for fields with an exponential semivariogram. We therefore calculate only the variance and the standard deviation of the variance for the fBm fields. We prefer to give the results of the statistical properties in terms of the integral to which the values would tend if we would have generated an infinite number of points in the finite field. In the most tedious situation, we obtain a quadruple integral which can be evaluated by standard numerical methods (Press and others, 1992, p. 161–164).

The variance $var(m)$ of the sample mean m (with autocorrelated values within the sample) can be obtained in many textbooks (Vanmarcke, 1983) and

can be derived as follows: without loss of generality we can here and in all the examples below consider the variable x_i translated with respect to the expected mean, that is $E[x] = 0$.

$$\begin{aligned} \text{var}(m) &= E \left[\left(\frac{1}{N} \sum_{i=1}^N x_i \right)^2 \right] = E \left[\frac{1}{N^2} \sum_{i=1}^N \sum_{j=1}^N x_i x_j \right] \\ &\approx \frac{1}{L^4} \int_0^L \int_0^L \int_0^L \int_0^L C(|\mathbf{r}_1 - \mathbf{r}_2|) dx_1 dx_2 dy_1 dy_2 \end{aligned} \quad (\text{B1})$$

where L is the length of the sample field and $\Delta x = \Delta y = L/\sqrt{N}$; we confine ourselves to 2-D square fields. We identify $E[x_i x_j] = C(|\mathbf{r}_i - \mathbf{r}_j|)$ as the autocorrelation function.

We can transform the integral in Equation (B1) to an integral over the unit square ($x_1 \rightarrow x_1/L$, etc.). We also can introduce radial coordinates (r) and solve analytically the integration toward r to reduce to a triple integral.

We proceed to sketch the derivation of the sample variance (var) of a finite field.

$$\begin{aligned} \text{var} &= E \left[\frac{1}{N} \sum_{i=1}^N \left(x_i - \frac{1}{N} \sum_{j=1}^N x_j \right)^2 \right] \\ &= E \left[\frac{1}{N} \sum_{i=1}^N x_i^2 - \frac{1}{N^2} \sum_{j=1}^N \sum_{k=1}^N x_j x_k \right] \\ &\approx \int_0^1 \int_0^1 \int_0^1 \int_0^1 \gamma(|\mathbf{r}_1 - \mathbf{r}_2|) dx_1 dx_2 dy_1 dy_2 \end{aligned}$$

We use the stationarity assumption and identified $\sigma^2 - E[x_i x_j] = \gamma(|\mathbf{r}_i - \mathbf{r}_j|)$ as the semivariogram. The variance is σ^2 . The integral can be reduced to a triple integral in exactly the same way as the given integral. The result is finite also for fBm fields.

Now we turn to evaluate the variance of the sample variance $\text{var}(\text{var})$.

$$\begin{aligned} \text{var}(\text{var}) &= E \left[\left(\frac{1}{N} \sum_{i=1}^N \left(x_i - \frac{1}{N} \sum_{j=1}^N x_j \right)^2 \right)^2 \right] - E^2 \left[\frac{1}{N} \left(\sum_{i=1}^N \left(x_i - \frac{1}{N} \sum_{j=1}^N x_j \right)^2 \right) \right] \\ &= \frac{1}{N^2} \sum_{i=1}^N \sum_{j=1}^N E[x_i^2 x_j^2] - \frac{2}{N^3} \sum_{i=1}^N \sum_{k=1}^N \sum_{l=1}^N E[x_i^2 x_k x_l] \\ &\quad + \frac{1}{N^4} \sum_{k=1}^N \sum_{l=1}^N \sum_{m=1}^N \sum_{n=1}^N E[x_k x_l x_m x_n] - \text{var}^2(x) \end{aligned}$$

We use the well-known relation for normal fields (Yang and Lake, 1989)

$$E[x_1x_2x_3x_4] = E[x_1x_2]E[x_3x_4] + E[x_1x_3]E[x_2x_4] + E[x_1x_4]E[x_2x_3]$$

and obtain

$$\begin{aligned} \text{var}(\text{var}) &= \frac{1}{N^2} \sum_{i=1}^N \sum_{j=1}^N E[x_i^2]E[x_j^2] + \frac{2}{N^2} \sum_{i=1}^N \sum_{j=1}^N E[x_ix_j]E[x_ix_j] \\ &\quad - \frac{2}{N^3} \sum_{i=1}^N \sum_{k=1}^N \sum_{l=1}^N E[x_i^2] E[x_kx_l] \\ &\quad - \frac{4}{N^3} \sum_{i=1}^N \sum_{k=1}^N \sum_{l=1}^N E[x_ix_k]E[x_lx_i] + \frac{3}{N^4} \sum_{k=1}^N \sum_{l=1}^N \sum_{m=1}^N \sum_{n=1}^N \\ &\quad E[x_kx_l]E[x_mx_n] - \text{var}^2(x) \end{aligned}$$

It is convenient to express the result in terms of the semivariogram γ rather than in terms of the autocorrelation function. After some algebraic manipulations entirely analogous to the procedures used, we obtain

$$\begin{aligned} \text{var}(\text{var}) &= 2 \int_0^1 \int_0^1 \int_0^1 \int_0^1 \gamma^2(|\mathbf{r}_1 - \mathbf{r}_2|) dx_1dx_2dy_1dy_2 - 4 \\ &\quad \cdot \int_0^1 \int_0^1 \int_0^1 \int_0^1 \int_0^1 \int_0^1 \gamma(|\mathbf{r}_1 - \mathbf{r}_2|) \\ &\quad \cdot \gamma(|\mathbf{r}_1 - \mathbf{r}_3|) dx_1dx_2dy_1dy_2dx_3dy_3 \\ &\quad + 3 \left(\int_0^1 \int_0^1 \int_0^1 \int_0^1 \gamma(|\mathbf{r}_1 - \mathbf{r}_2|) dx_1dx_2dy_1dy_2 \right)^2 \end{aligned}$$

The sixfold integral can be reduced to a quadruple integral by using cylindrical coordinates and the analytical solution of the radial dependent part.

APPENDIX C: 2-D SPECTRAL DENSITY FUNCTION FOR fBm

We only sketch the derivation of S_2 as the detailed derivation for fBm has been described extensively elsewhere (Bruining, 1992). The procedure is to determine first the 1-D spectral density function $S_1(\omega)$ as the Fourier cosine transform of the covariance function $C(s)$ (Vanmarcke, 1983)

$$S_1(\omega) = \frac{1}{\pi} \int_0^\infty C(s) \cos(\omega s) ds \tag{C1}$$

Subsequently we use Equation (C-4), proposed by Tsuji (1955), to transform $S_1(\omega)$ to the 2-D spectral-density function $S_2(\omega)$. For second-order stationary fields the covariance function $C(s)$ is the variance minus the variogram $\gamma(s)$, both of which are assumed to be known. Here we denote the lag-distance by s . For fBm, the variogram function is $\gamma(s) = \gamma_o s^{2H}$ where γ_o is a variance parameter (the variogram at $s = 1$) and H is the Hurst or intermittency coefficient. The variance is infinite because $\gamma(s)$ increases without bound as s increases. However, if we define the variance as the limit of γ as R approaches infinity, we can write the covariance function as

$$C(s) = \lim_{R \rightarrow \infty} \gamma_o R^{2H} - \gamma_o s^{2H} \quad (\text{fBm}) \quad (\text{C2})$$

In spite of the infinite term in Equation (C2) expressions for the spectral density functions are bounded. Indeed, substitution into Equation (C1) leads, after partial integration, the cancelling of two identical terms (which tend to infinity) and the use of Abramowitz and Stegun (1972) to simplify the relevant mathematical functions, to the following expression of the 1-D spectral density function.

$$S_1(\omega) = \frac{H\gamma_o}{\Gamma(1-2H) \cos(H\pi)} \frac{1}{\omega^{2H+1}} \quad (\text{fBm}) \quad (\text{C3})$$

The 1-D spectral density function $S_1(\omega)$ can be transformed to the 2-D spectral density function $S_2(\omega)$ (Tsuji, 1955).

$$S_2(\omega) = \frac{1}{\pi} \int_{\omega}^{\infty} \frac{d}{d\omega_1} \left(\frac{1}{\omega_1} \frac{d}{d\omega_1} S_1(\omega_1) \right) \sqrt{\omega_1^2 - \omega^2} d\omega_1 \quad (\text{C4})$$

Substitution of Equation (C3) and some tedious algebra lead to an integral that can be evaluated by comparison to an integral given by Gradshteyn and Ryzhik (1979) [p. 285, eq. (3)]. Using the properties of the gamma-function (Abramowitz and Stegun, 1972) leads to a simple expression for the 2-D spectral density function for fBm

$$S_2(\omega) = \frac{H^2 \gamma_o^2 2^{2H}}{\pi^2} \frac{\Gamma(H)^2 \sin(H\pi)}{\omega^{2H+2}} \quad (\text{C5})$$

APPENDIX D. 2-D SPECTRAL-DENSITY FUNCTION FOR fGn

$S_1(\omega) = 2H\gamma_o(1 - \cos(\omega\delta))/(\pi\delta^2\omega^{2H+1})\Gamma(2H)\sin(H\pi)$ into Eq. (C4) to obtain the 2-D spectral density function for fGn is rather unwieldy. Consequently its numerical evaluation may give rise to some intricate problems. Therefore, we here give not only the full expression but also some limiting expansions. We use Abramowitz and Stegun (1972), Gradshteyn and Ryzhik (1979), Prudnikov, Brychkov, and Marichev (1986), and Oberhettinger (1990) to determine

and simplify the relevant analytical expressions. The full expression for the 2-D spectral density function for fGn reads

$$\begin{aligned}
 S_2(\omega) = & \frac{2H\gamma_o\Gamma(2H)\sin(H\pi)}{\pi^2} \left(\frac{\sqrt{\pi}\Gamma(H+1)}{\delta^2\Gamma(H+\frac{1}{2})\omega^{2H+2}} \right. \\
 & - \frac{1}{\delta\omega^{2H+1}} \left(\frac{\omega\delta}{2} B\left(\frac{1}{2}, H\right) {}_1F_2\left(\frac{1}{2}-H; 1-H, \frac{3}{2}; \frac{-\omega^2\delta^2}{4}\right) \right. \\
 & + \left. \frac{\sqrt{\pi}}{2} \left(\frac{\omega\delta}{2}\right)^{2H+1} \frac{\Gamma(-H)}{\Gamma(H+\frac{3}{2})} {}_1F_2\left(\frac{1}{2}; H+\frac{3}{2}, H+1; \frac{-\omega^2\delta^2}{4}\right) \right) \\
 & - \frac{2H+1}{\delta^2\omega^{2H+2}} \left(\frac{1}{2} B\left(\frac{1}{2}, H+1\right) {}_1F_2\left(-\frac{1}{2}-H; -H, \frac{1}{2}; \frac{-\omega^2\delta^2}{4}\right) \right. \\
 & + \left. \frac{\sqrt{\pi}}{2} \left(\frac{\omega\delta}{2}\right)^{2H+1} \frac{\Gamma(-H-1)}{\Gamma(H+\frac{3}{2})} {}_1F_2\left(\frac{1}{2}; H+2, H+\frac{3}{2}; \frac{-\omega^2\delta^2}{4}\right) \right) \Big) \tag{D1}
 \end{aligned}$$

The equation uses the beta function $B(\mu, \nu) = \Gamma(\mu)\Gamma(\nu)/\Gamma(\mu + \nu)$. It also uses the hypergeometric function ${}_1F_2(a; b, c; z) = \sum_0^\infty (a)_k z^k / ((b)_k(c)_k k!)$ with the definition $(a)_n = a(a+1)(a+2) \dots (a+n-1)$ and $(a)_0 = 1$. The function must not be confused with the Gauss hypergeometric function ${}_2F_1(a, b; c; z) = \sum_0^\infty (a)_k (b)_k z^k / ((c)_k k!)$ (see Abramowitz and Stegun, 1972).

The numerical evaluation of Equation (D1) can be achieved by substituting the first 40 terms of the sum that represents the hypergeometric series. Round-off errors will dominate the numerical evaluation unless one notes that the first term cancels with the leading part of the fourth term, that is

$$- \frac{2H+1}{\delta^2\omega^{2H+2}} \frac{1}{2} B\left(\frac{1}{2}, H+1\right) (1 + \text{h.o.t.})$$

It can be shown that the expression (D1) for low frequencies ($\omega \ll 1/\delta$) reduces to the spectral density function obtained from the autocovariance function of fGn for $\delta \rightarrow 0$, that is

$$\begin{aligned}
 \lim_{\delta \rightarrow 0} C(s, \delta) &= \lim_{\delta \rightarrow 0} \frac{\gamma_o}{2\delta^2} ((s + \delta)^{2H} - 2s^{2H} + |s - \delta|^{2H}) \\
 &= \gamma_o H(2H - 1) s^{2H-2}
 \end{aligned}$$

The application of the procedure as used here gives the following expressions of the 2-D spectral-density function for fGn in the limit that $\delta \rightarrow 0$.

$$\lim_{\delta \rightarrow 0} S_2(\omega, \delta) = \frac{H\gamma_o \Gamma(2H) \sin(H\pi)}{\sqrt{\pi^3}} \frac{\Gamma(H)}{\Gamma(H - \frac{1}{2}) \omega^{2H}}$$

It is not easy to prove whether the spectral-density function given by Equation (D1) for finite values of the smoothing parameter δ is always positive. In the numerical evaluation negative values do occur, which formally indicates that fGn is not a viable model in 2-D (Vanmarcke, 1983, p. 105). In Appendix E, we argue that in spite of this in practice fGn can be used as a 2-D and 3-D heterogeneity model.

APPENDIX E. 3-D SPECTRAL DENSITY FUNCTIONS

Perhaps contrary to intuition, the derivation of a 3-D spectral density function is easier than the derivation of a 2-D spectral density function (Tsuji, 1955), that is

$$S_3(\omega) = -\frac{1}{2\pi\omega} \left\{ \frac{dS_1(\omega_1)}{d\omega_1} \right\}_{\omega_1=\omega} \quad (\text{E1})$$

Equation (E1) can be evaluated easily for fBm and fGn and yields

$$S_3(\omega) = \frac{H\gamma_o}{2\pi\Gamma(1-2H) \cos(H\pi)} \frac{2H+1}{\omega^{2H+3}} \quad (\text{fBm})$$

and

$$S_3(\omega) = \frac{H\gamma_o}{\pi^2} \Gamma(2H) \sin(H\pi) \cdot \frac{(2H+1)(1 - \cos(\omega\delta)) + \omega\delta \sin(\omega\delta)}{\delta^2} \frac{1}{\omega^{2H+3}} \quad (\text{fGn}) \quad (\text{E2})$$

Equation (E2) shows that, formally, fGn with a finite value of the smoothing parameter δ cannot be used as a 3-D heterogeneity model because the spectral density function can become negative as $\omega \gg 1/\delta$ (see Vanmarcke, 1983, p. 105).

For many practical purposes, the frequency components $\omega \gg 1/\delta$ add detail for scales smaller than the smoothing parameter δ and thus have no physical meaning. Hence, in practice, one can use Equation (E2) up to a frequency where $S_3(\omega)$ becomes zero to obtain the low-frequency part of the 3-D spectral-density function for fGn, and assume that the high-frequency part of the 3-D spectral-density function is zero. Other arguments in favor of the practical (formally erroneous) approach is that (i) fGn with $\delta \rightarrow 0$ also can be used as a 3-D model and (ii) there is some arbitrariness in the use of the smoothing parameter which is introduced essentially to define fGn as some type of derivative of fBm.